Class 0 Source CARMA-7 in Serpens South

Makoto A. Johnstone [1] and Adele L. Plunkett [2]

[1] *Middlebury College, 14 Old Chapel Rd, Middlebury, VT 05753, USA*
[2] *National Radio Astronomy Observatory (NRAO), 520 Edgemont Road, Charlottesville, VA 22903, USA*

ABSTRACT

Previous observations of the low mass Class 0 protostar, CARMA-7, in the Serpens South cluster region detected outflow ejection events traced by ^{12}CO $J = 2 \rightarrow 1$. However, little is known about the molecular abundances and morphologies of molecular lines other than carbon monoxide isotopologues. We present follow-up observations of 9 molecular emission lines near CARMA-7 using the Atacama Large Millimeter/sub-millimeter Array. We confirm the presence of a bipolar outflow extending in the north-south direction with a position angle of $4°$ as traced by ^{12}CO $J = 2 \rightarrow 1$, H_2CO $3(0,3) - 2(0,2)$, and H_2CO $3(2,1) - 2(2,0)$. Further investigation of the H_2CO and c-C_3H_2 lines uncovered a low velocity extended emission feature slanted to the southwest with a position angle of $72°$. We interpret this feature as a potential accretion flow, but further analysis via modeling is necessary. The $C^{18}O$ $2 \rightarrow 1$ emission line shows early signs of Keplerian rotation in the disk/envelope. However, other known disk and envelope tracers such as ^{13}CO, N_2D^+, and H_2CO fail to show signs of rotation. We find that CARMA-7 does not hold a disk larger than 305 AU and that the detection of a strong outflow is not a clear indicator of an evolved rotating disk.

Keywords: stars: formation, stars: protostars, ISM: molecules, ISM: individual (CARMA-7)

1. INTRODUCTION

1.1. *Early Star Formation*

The formation of low-mass stars begins with the gravitational collapse of dense molecular cloud cores (Froebrich et al. 2006; Larson 2003). As the core collapses, the surrounding gas spins due to the non-zero angular momentum, eventually causing it to flatten and form into a dense rotating protostellar disk. As the protostar continues to accrete mass from the infalling envelope of dust and gas, the excess angular momentum is released by bipolar jets of gas, known as molecular outflows, that launch out of the core (Froebrich et al. 2006; Larson 2003).

Class 0 protostars are in this main accretion stage, characterized by high velocity jets and a developing disk embedded in a massive envelope. Their energetic molecular outflows are driven by accretion events via the disk, and therefore, are potential indicators of protostellar accretion. Analyzing the properties of outflow gas tracers and envelope/disk gas tracers could provide insight on the unique physical features of young protostars, as well as the correlations between outflow ejection events and accretion events.

1.2. *Serpens South and CARMA-7*

Our source, CARMA-7, is a class 0 protostar located 436 parsecs (pc) from earth and is the brightest millimeter continuum source in the Serpens South cluster region (Plunkett et al. 2018). A previous study, Plunkett et al. (2015), observed $J = 2 \rightarrow 1$ emission lines of carbon monoxide isotopologues (^{12}CO, C^{18}O, ^{13}CO) near CARMA-7. ^{12}CO traced molecular outflows in the north-south direction (position angle: $4°$) and revealed distinct knots of gas along the outflow axis (Plunkett et al. 2015). This unambiguous emission feature implies the occurrence of episodic ejection events, raising new questions about the outflow ejection mechanism.

The molecular gas properties of CARMA-7 provide insight on the physical features of the protostellar system and its chemical complexity. In this report, we examine 9 molecular lines near CARMA-7 and distinguish molecular detections into 3 categories: 1) outflow gas tracers, 2) disk/envelope tracers, and 3) other.

This paper is organized in the following manner. We present the conducted observations Section 2, and the data analysis methods are listed in Section 3. In Section 4, we present the morphology and molecular abundances of the observed molecular lines. We report our interpre-

tations of the identified emission features in Section 5. Lastly, in Section 6, we summarize our findings and final categorizations of molecular gas tracers.

2. OBSERVATIONS

2.1. *Molecular Line Observations*

Here, we present Band 6 observations of CARMA-7 from ALMA project 2019.1.00912.S. 9 molecular emission lines listed in Table 1 were observed. With angular resolutions ranging from 0.14" to 0.7", these observations resolve features greater than approximately 305 astronomical units (AU) in size.

Table 1. Observed Spectral Lines

Spectral Window	Rest Frequency (GHz)
N_2D^+ $J = 3 \to 2$	231.321828
^{13}CS v=0 $2 \to 1$	231.220686
^{12}CO v=0 $2 \to 1$	230.538000
H_2CO 3(0,3)-2(0,2)	218.222192
c-C_3H_2 v=0 6(1,6)-5(0,5)	217.822148
DCN 0 $J = 3 \to 2$	217.238530
^{13}CO v=0 $2 \to 1$	220.398684
$C^{18}O$ $2 \to 1$	219.560358
H_2CO 3(2,1)-2(2,0)	218.760066

3. DATA ANALYSIS

3.1. *Moment Maps*

Images cubes for each molecular line were visualized using the Cube Analysis and Rendering Tool for Astronomy (CARTA) Software. Using the contour feature, frequency channels with emission intensity greater than 3 times the root-mean-square (rms) noise level were identified.

Moment 0 maps were created for each spectral line by integrating the flux across all channels with identified emission. This process was conducted via SpectralCube, a Python package designed to analyze 3-dimensional astrophysical data cubes. For moment 1 maps, a mask of 3 rms was applied to the image cube, and the SpectralCube package was utilized to calculate the velocity-weighted intensity. The moment maps in this paper display the moment 1 values using color maps and moment 0 is shown in contours. For ease of interpretation, the moment 1 color map was limited to within the moment 0 contours.

3.2. *Channel Maps*

Channels with unique emission features were identified via CARTA and plotted individually with Python

using the matplotlib package. Beam dimensions were converted to pixels to plot the beam size.

3.3. *Position-Velocity Diagrams*

Position Velocity diagrams were created via pvextractor, a Python package used to extract position-velocity slices from data cubes. The path of the slice was determined based on the desired position angle. To analyze outflow gas features, slices were made directly along the outflow axis. For disk gas features, the slice was made perpendicular to the outflow axis, an admittedly naive estimate of the location of the disk. Slices had a length of 12" centered about the source and at widths between 0.5" and 2.0".

3.4. *Dynamic Timescales*

Time scales of potential outflow-tracing molecular emission were calculated by visually identifying the most extended emission in each velocity channel. By inputting the the offset of the emission relative to the central source, and the source distance from earth (436 pc), the estimated physical distance traveled by the ejecta was calculated via the Small Angle Formula:

$$\theta_{arcseconds} = 206265 \frac{d}{D} \tag{1}$$

where $\theta_{arcseconds}$ is the offset in arcseconds, D is the distance to the object, and d is the physical separation or in this case, the distance traveled by the ejecta. The calculated distance traveled was then divided by the velocity of the channel map relative to the rest velocity (- V_{LSR}|), and this process was repeated in all channels with emission intensity greater than 3σ. These timescales were computed under the assumption that ejecta were launched from the source, CARMA-7.

Each channel represents the emission summed over a velocity range of approximately 0.16 km/s, meaning that the velocity used to compute the dynamic timescale is not the exact velocity of the identified emission. Additionally, the most extended emission was identified by eye, having an uncertainty of about 1 to 2 pixels (0.01" to 0.02"). These potential sources of error must be considered when inspecting the data.

4. RESULTS

4.1. *Envelope and Disk*

We estimate the rotating disk to be oriented perpendicular to the primary outflow, at approximately 94° counterclockwise to the vertical. Figure 1 presents the position-velocity diagram of the $C^{18}O$ line sliced along this assumed direction of the disk (positon angle: 94°).

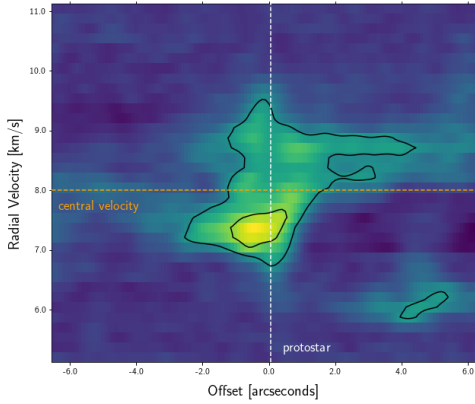The emission velocity peaks near the central source at |OFFSET| $\approx$ 0. The emission is slightly elongated

Figure 1. C^{18}O Position-Velocity Diagram Perpendicular to Outflow Axis a) A slice with a length of 12" and a width of approximately 0.5" was made perpendicular to the outflow axes at 94°. Contours show levels of 3σ of position-velocity intensity. Cloud central velocity ($V_c = 8$ km/s) is marked by an orange dashed line. Likewise, the location of the protostar (OFFSET = 0) is marked by a white dashed line. A hyperbolic velocity gradient is shown, most visible in the bottom right quadrant.

in east-west direction, and the velocity gradient curves are faintly hyperbolic as it extends. Though unresolved, these curves may be indicators of Keplerian rotation in the developing disk.

4.2. *Outflow Cavity Walls*

As the outflow travels through the cavity, the energetic jets of gas push envelope material against the cavity wall, resulting in the accumulation of low velocity gas (Tychoniec et al. 2021). The morphology of outflow tracers and outflow cavity wall tracers are similar in that they both extend along the outflow axis, however, emission along the cavity walls curve into a distinctive wide U-shape (Tychoniec et al. 2021).

These features are apparent in c-C$_3$H$_2$ moment map (Figure 2). The U-shape associated with cavity wall tracers is seen in the inner moment 0 contours. Emission of intensity stronger than 3σ was detected at low velocities ($|V_c - V_{LSR}| \leq 2.2$ km/s). The emission is more extended in the northeast-southeast direction, and this asymmetrical morphology may be attributed to an asymmetrical envelope, a likely possibility considering the young age of the source.

4.3. *Outflows and Extended emission*

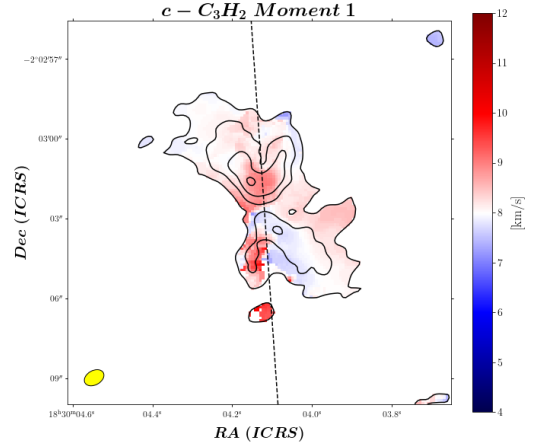Figure 3 presents moment maps for ^{12}CO and the two H$_2$CO transitions centered around CARMA-7. The

Figure 2. Moment 0 and 1 map of c-C$_3$H$_2$. Moment 0 map is in black contours, marking 3σ levels. The dashed black line indicates the outflow axis (position angle 4°) Emission features are at low velocities, and are primarily in the north-south direction with slight elongation to the east and west.

emission features for both molecular lines extend in the north-south direction and agree with previously reported outflow axis with the position angle of 4° (Plunkett et al. 2015).

The ^{12}CO emission is optically thick and traces distinct bipolar lobes at high velocities, with the red-shifted emission extending northward and the blue-shifted emission extending southward (Figure 3). The emission features appear clumpy, particularly in the northern lobe, resembling the knots of ejecta reported in Plunkett et al. (2015) (Figure 3).

The H$_2$CO 3(0,3)-2(0,2) emission also extends along the outflow axis, but the structure is complex. Although the northern emission features are predominantly red-shifted, features to the south alternate between red-shifted and blueshifted emission. (Figure 3). The emission of H$_2$CO 3(2,1)-2(2,0), the other observed H$_2$CO transition line, is compact but displays similar alternating emission features.

Further inspection via channel maps revealed that the H$_2$CO 3(0,3)-2(0,2) emission stretches in the east-west direction at low velocities, most notable at 8.83 km/s and 8.66 km/s (Figure 4). The extended emission resembles an outflow, but the feature is only present in low velocity red-shifted channels, raising the possibility that this may be infall gas.

c-C$_3$H$_2$ emission features in this velocity range were examined to look for signs of an outflow cavity. Figure 5 shows the integrated intensity of H$_2$CO 3(0,3)-2(0,2)
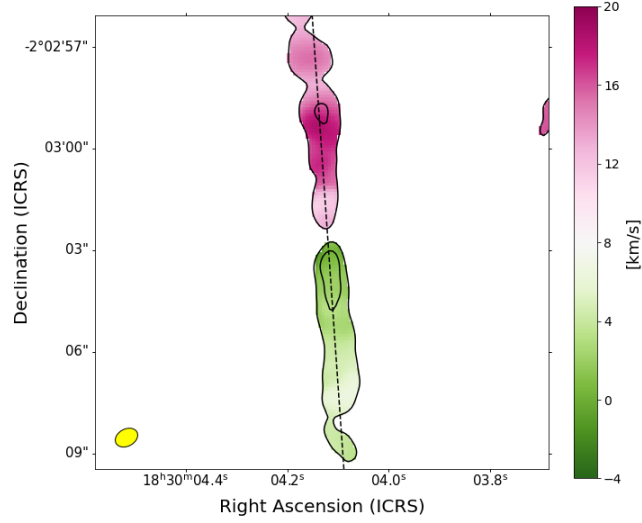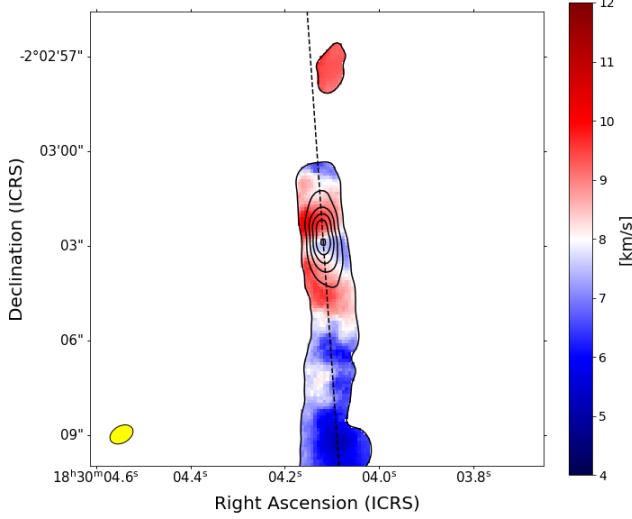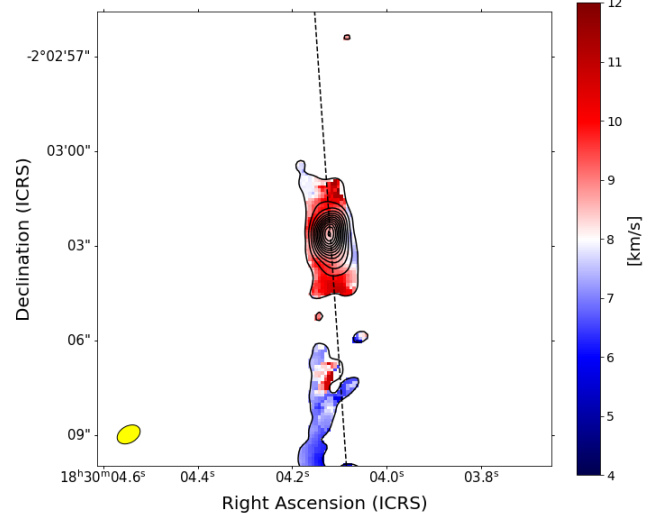
(a) ^{12}CO Moment 1

(b) H$_2$CO 3(0,3)-2(0,2) Moment 1

(c) H$_2$CO 3(2,1)-2(2,0) Moment 1

Figure 3. Moment 0 and 1 maps of ^{12}CO and H$_2$CO lines, centered at class 0 protostar CARMA-7. Moment 0 map is in black contours, showing 3σ levels. Emission features extend in the north-south direction. The dashed black line indicates the outflow axis (position angle $4°$). Northern (southern) emission features are predominantly red-shifted (blue-shifted) and are shown in pink and red (green and blue). The color map difference accounts for the change in velocity scale. Beam size is indicated in yellow on the bottom left corner of both moment maps.
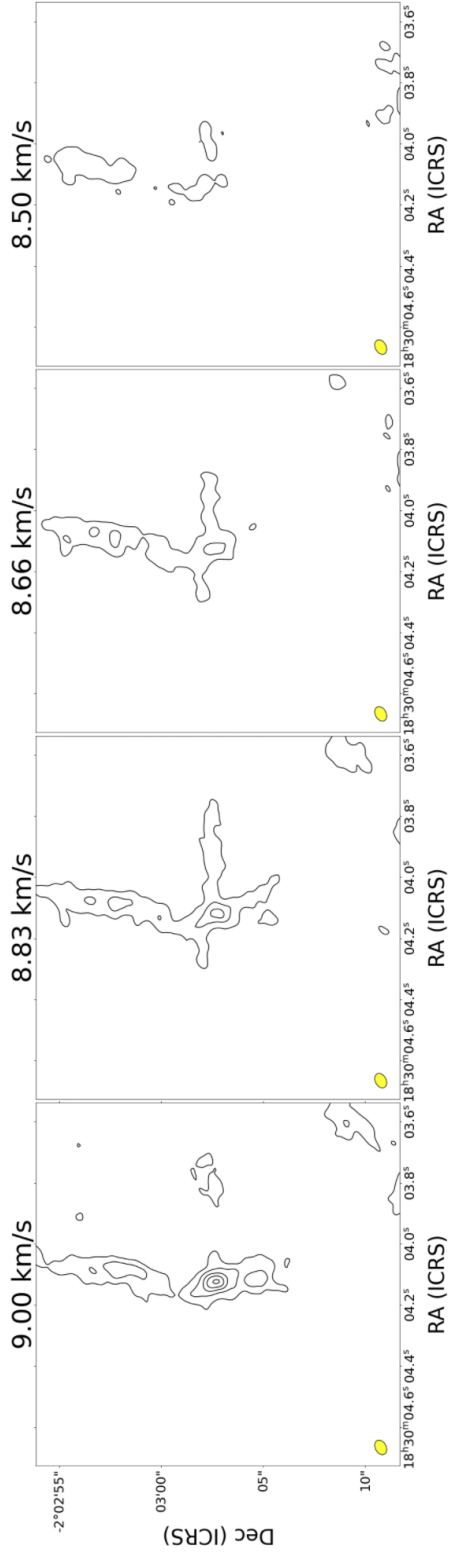
Figure 4. Channel maps for H$_2$CO 3(0,3)–2(0,2). Black contours are 3 rms and increment by 3. Each plot represents the integrated emission intensity across a velocity range of approximately 0.167 km/s centered about the velocity specified above each plot. Beam size is shown in yellow at the bottom left corner of each channel map.
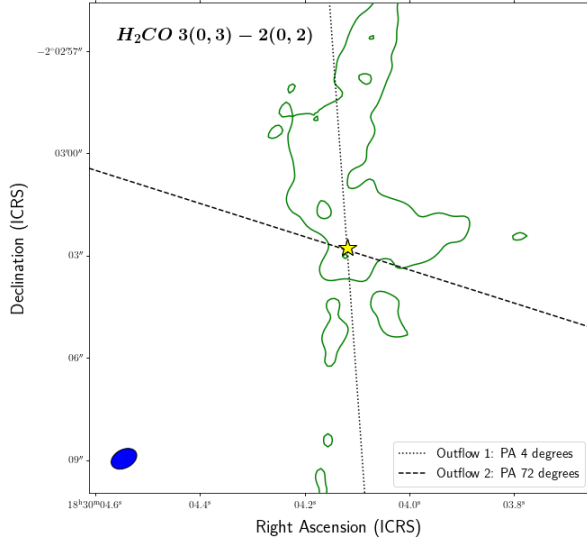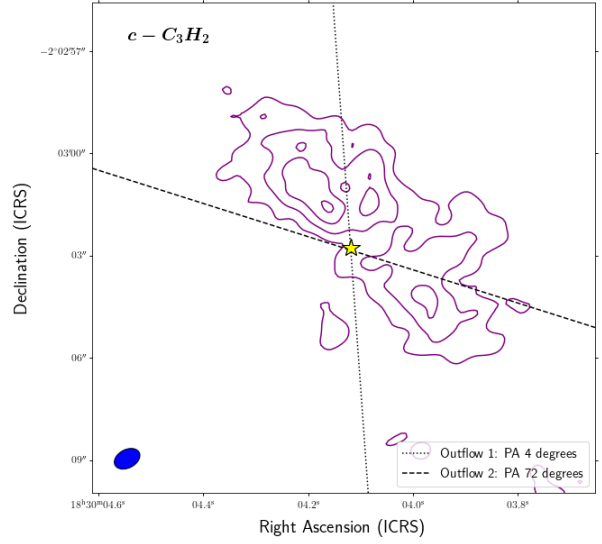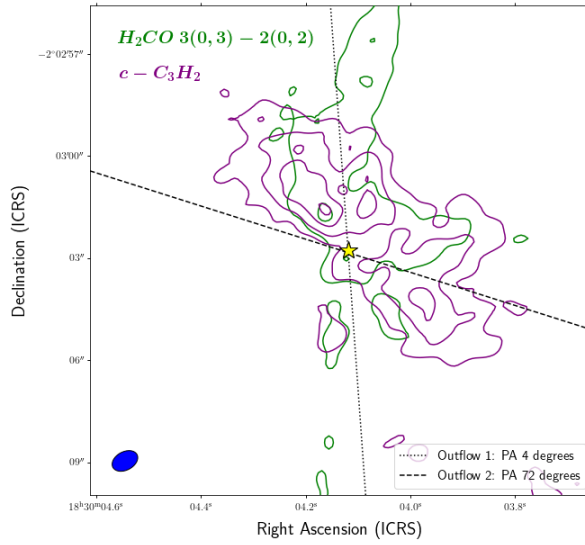
(a) Low Velocity H_2CO 3(0,3)-2(0,2)

(b) Low Velocity c-C_3H_2

(c) Low Velocity H_2CO 3(0,3)-2(0,2) (green) and
c-C_3H_2 (purple)

Figure 5. Integrated Intensity at Low Velocities (8 km/s to 9 km/s) for H_2CO 3(0,3)-2(0,2) and c-C_3H_2. Contours are 3σ and increment by $3sigma$. Integrated intensity is shown in green contours show for H_2CO 3(0,3)-2(0,2), and in purple contours for c-C_3H_2). Potential outflow axes are marked with dashed and dotted black lines. Contours for both molecular lines are overlaid in **(c)**. Extended emission features to the west overlap.

and c-C_3H_2 across the 8 km/s to 9 km/s range. The characteristic U-shape in the inner contours of C_3H_2 tilts to the southwest, revealing an outflow cavity wall-like structure that is also traced by the extended emission seen in the H_2CO lines (Figure 5). We estimate a 72° position angle for this potential secondary axis shown by the dashed line in Figure 5.

Figure 6 presents position-velocity (PV) diagrams of H_2CO 3(0,3)-2(0,2) sliced along the primary outflow axis (position angle: 4°) and the potential secondary axis (position angle: 72°) (hereafter Axis 1 and Axis 2 respectively). Both PV diagrams show high intensity and high velocity emission at offsets less than 2" from the protostar (Figure 6), a feature associated with infall motion.

Differences in the PV diagrams arise at larger offsets. The PV diagram for Axis 1 show peaks in relative velocity ($|V_c - V_{LSR}|$) at larger distances from the source (Figure 6). This velocity gradient is associated with outflow ejection features. The PV diagram for Axis 2 shows low velocity extended emission to the left, but the emission features are approximately symmetrical about the orange horizontal line representing V_c. These parallelisms are not characteristic of outflow gas.

The time scales of emission along the two axes are shown in Figure 7. Here, we assume that emission was ejected from the source along each of the axes. The timescales of redshifted emission for Axis 1 coincide with the Axis 2 emission (most notably at OFFSET < 4"), and their dynamic timescales increase with distance (Figure 7). The blueshifted emission for Axis 1 shows the opposite trend. The data reveals a negative trend line in the timescales, indicating that more recent ejecta are present at larger offsets (Figure 7).

Despite the differences in their trends, the age of the ejecta along the two axes overlap (Figure 7), revealing that if there were to be secondary outflow feature along Axis 2, the two outflows would have been active simultaneously within the past 20,000 years. These results will be discussed further in Section 5.2.

4.4. Compact Emission

Figure 8 presents moment maps for N_2D^+, ^{13}CO, DCN, and ^{13}CS.

N_2D^+ and ^{13}CO have faint blue-shifted emission features concentrated at the source (Figure 8). The ^{13}CO moment map shows a segment of extended blue-shifted emission to the bottom right of the plot, but this may be attributed to CARMA-6, a neighboring Class 0 protostar located south-west of CARMA-7 (Plunkett et al. 2015) (Figure 8). The low abundance of N_2D^+ and ^{13}CO was unexpected, given that both are known envelope

tracers (Tychoniec et al. 2021). The lack of red-shifted emission is also peculiar in that an accretion disk would harbor redshifted counterparts to blueshifted emission as it rotates about the core.

DCN and ^{13}CS are slightly elongated along the outflow axis but are otherwise compact. DCN emission features are high intensity and primarily red-shifted. The ^{13}CS moment 1 map show both red-shifted and blueshifted emission, but the physical size of the moment 1 features is small (approximately 420 Au).

Our observations resolve images of physical sizes greater than approximately 305 Au. Given that these compact emission features have physical sizes as small as 210 Au (N_2D^+), we must acknowledge that these images are unresolved, and we are unable to make definitive conclusions about the morphology of the gas- an admittedly disappointing result.

5. DISCUSSION

5.1. Keplerian Disk Rotation

The kinematics of the $C^{18}O$ emission demonstrate early signs of Keplerian disk rotation (Figure 6). Upon visual inspection, the velocity gradient appears hyperbolic, agreeing with the equation:

$$\frac{v^2}{r} = \frac{GM}{r^2} \tag{2}$$

where

$$v \propto \frac{1}{\sqrt{r}} \tag{3}$$

Here, v is the velocity of the emission, r is the offset/distance from the source, M is the protostellar mass, and G is the gravitational constant (Maret et al. 2020). However, we are unable to compute the exact rotation curve because the mass of the protostar (M) is unknown. Future steps will require modeling the rotation curve using the $C^{18}O$ detections to estimate the central mass.

5.2. Extended Emission: Outflow or Streamer?

The extended H_2CO emission in the 8 km/s to 9 km/s range presented the possibility of a secondary outflow structure (Figure 4). Examining c-C_3H_2 moment 0 contours within that velocity range confirms the presence of a cavity in the southwest at position angle 72° that corresponds to the extended H_2CO emission (Figure 5).

Okoda et al. (2021) reports similar emission features in the H_2CO line, showing a secondary outflow perpendicular to the primary outflow at low velocities in another Class 0 protostar- IRAS 153983359. They propose that this secondary outflow structure is the remnant of an older jet that is no longer active. The emission is only detected at low velocities because the faster components
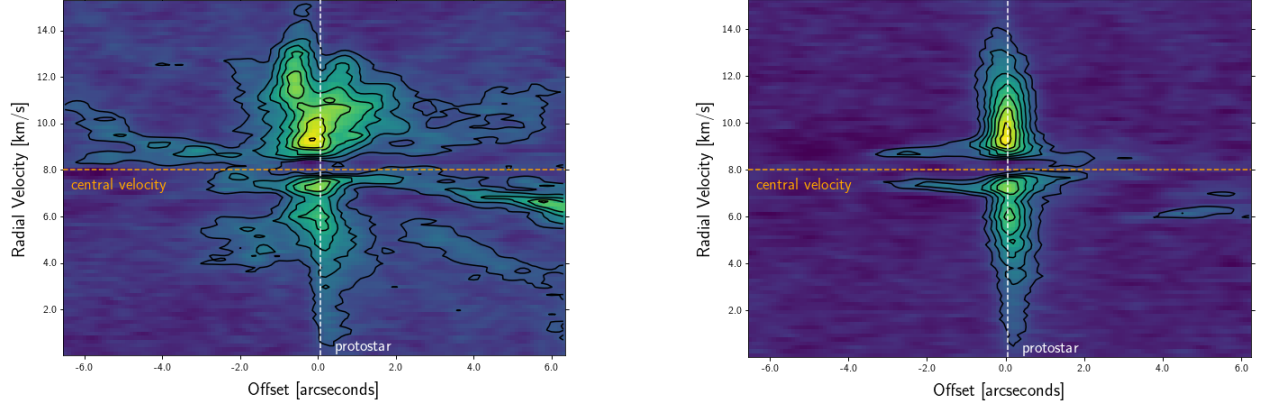
(a) Axis 1: 4° Position Angle

(b) Axis 2: 72° Position Angle

Figure 6. H$_2$CO 3(0,3)-2(0,2) Position-Velocity Diagrams Along Potential Outflow Axes. Position Velocity diagrams were sliced along the outflow axes at position angles, 4° and 72° respectively. Slice width is approximately 0.5". Contours show levels of 3σ of position-velocity intensity. Cloud central velocity ($V_c = 8$ km/s) is marked by an orange dashed line. Likewise, the location of the protostar (OFFSET = 0) is marked by a white dashed line.
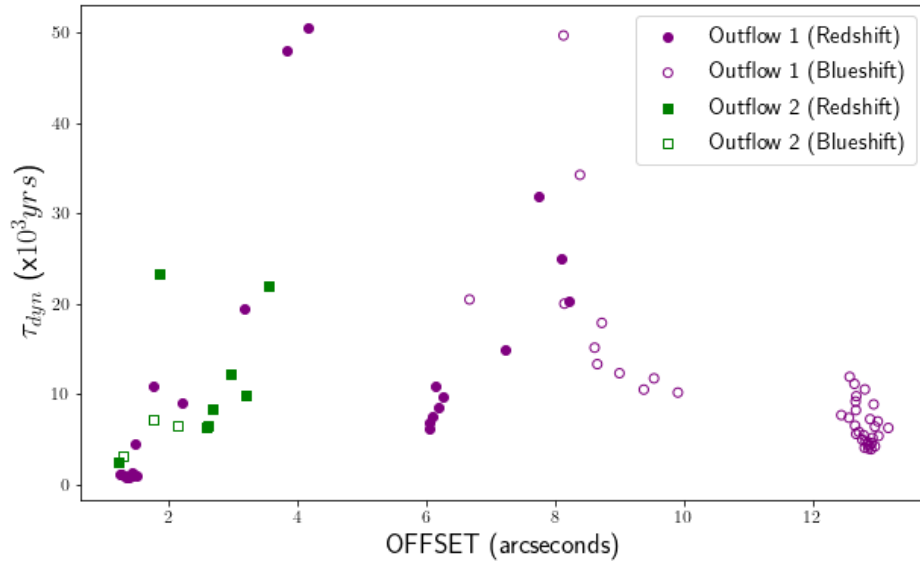

Figure 7. Dynamic Timescales of H2CO 3(0,3)-2(0,2) Emission. Timescales are not corrected for incline (i). Green (purple) markers indicate dynamic timescales for emission along Axis 1 (Axis 2). Filled (unfilled) in markers represent redshifted (blueshifted) emission.
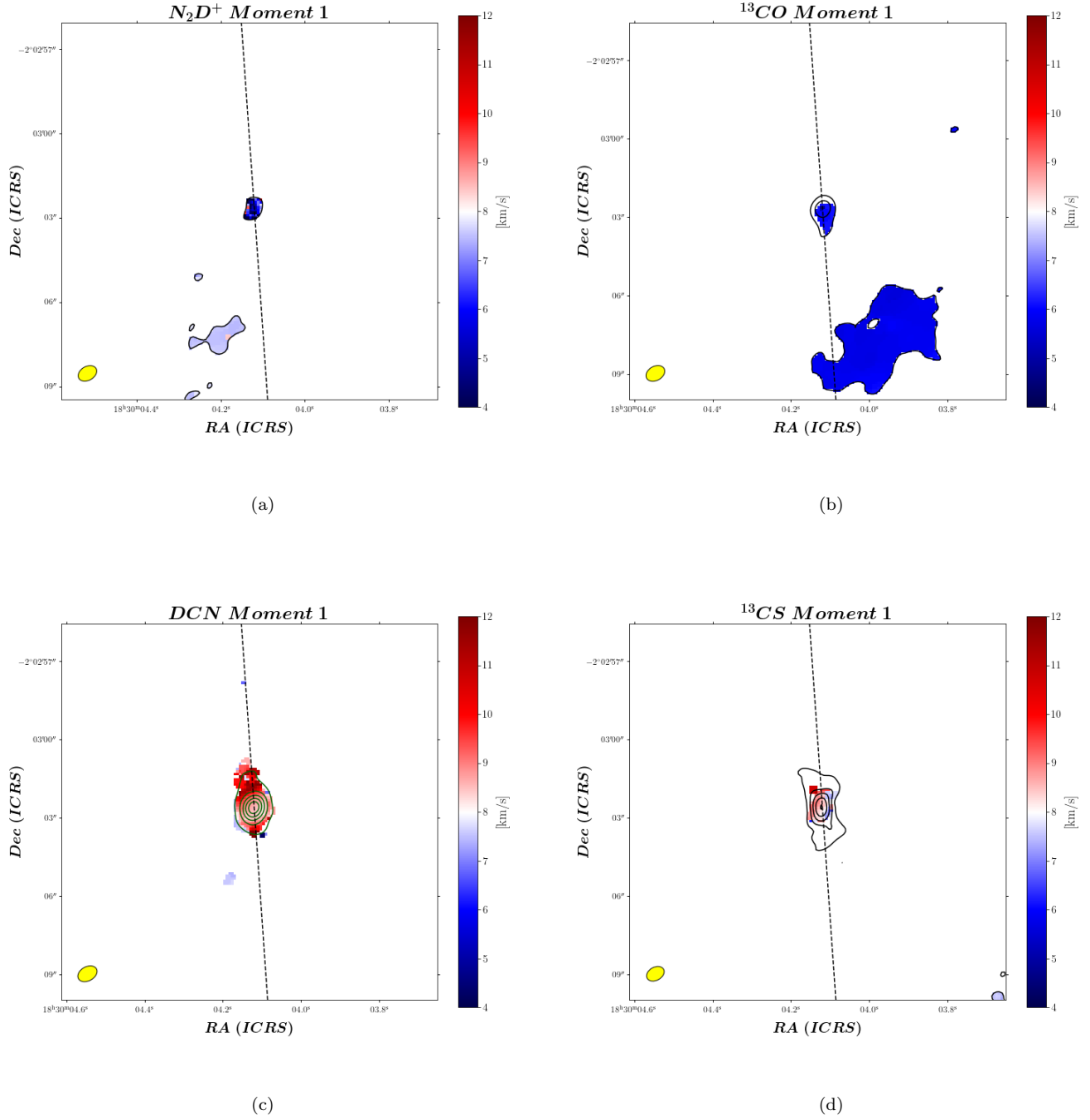
(a)

(b)

(c)

(d)

Figure 8. Moment 0 and 1 map of a) N_2D^+, b) ^{13}CO, c) DCN, and d) ^{13}CS. Moment 0 map is in black contours, showing 3σ levels. Note that the contours for DCN are in green, signifying a higher intensity starting at 5σ and incrementing by 10σ. The dashed black line indicates the known outflow axis (position angle $4°$) Emission features are compact with minimal extension along the axis.

have been dissipated by the envelope gas (Okoda et al. 2021).

This theory explains why the extended emission is only present with 1 km/s of the systemic cloud velocity ($V_c = 8.0$ km/s). However, the computed timescales reveal that if the extended feature is a secondary outflow, the two outflows would have been active simultaneously within the past 20,000 years.

A more likely possibility is that the extended emission feature is an accretion flow, a spiral-like stream of material that connect the envelope to the disk. These streamers have been identified in other Class 0 protostars such as VLA1623 and IRAS 03292+3039 (Hsieh et al. 2020; Pineda et al. 2020). Infall gas close to the source agrees with the systemic cloud velocity ($V_c = 8.0$ km/s) which explains our low velocity detections (Hsieh et al. 2020).

Previous studies have reported $C^{18}O$, ^{13}CO, SO, HCO^+, and HC_3N as accretion flow tracers (Pineda et al. 2020; Yen et al. 2014; Yen et al. 2017). Observations of SO, HCO^+, and HC_3N may be necessary to confirm the origins of the extended emission feature. Dendrogram analysis to identify features surrounding the disk in the position-position-velocity (PPV) space (Hsieh et al. 2020; Rosolowsky et al. 2008), as well as accretion flow modeling are potential next steps in further investigating potential streamers.

5.3. *Low Abundance of Disk Tracers*
5.3.1. *N_2D^+*

Gas phase CO destroys N_2D^+, and therefore, N_2D^+ detections correlate with depletions in gaseous CO (Tychoniec et al. 2021). Thus, N_2D^+ is known to be present in the cold dense envelope where the freeze-out of gaseous CO onto grain surfaces occurs as temperatures fall below 20K (Sandford & Allamandola 1993; Tychoniec et al. 2021). In the warm inner envelope surrounding the core, however, temperatures rise to above 100K, and CO is vaporized off of the dust grains (Tychoniec et al. 2021). Here, N_2D^+ detections are unexpected, yet our data finds N_2D^+ emission concentrated at the central source.

Given that the detected emission features contradict known chemical properties of N_2D^+, we believe this may be a misdetection and that we are detecting gas from molecules with emission frequencies similar to that of N_2D^+. Nevertheless, follow-up observations may be necessary to reexamine the reliability of our detections.

5.3.2. *^{13}CO*

Our detections of ^{13}CO are faint and compact (Figure 8). The low abundance of ^{13}CO is unexpected given that

^{13}CO is a known inner envelope and disk tracer that has been used to identify disk rotation in Class 0 protostars (Tychoniec et al. 2021; Tobin et al. 2012; Maret et al. 2020).

The low abundance of ^{13}CO could be explained by the young age of CARMA-7. It is difficult to analyze the small accretion disks in Class 0 sources because it is hidden behind envelope emission (Tychoniec et al. 2021). Furthermore, Class 0 sources have lower $^{13}CO/C^{18}O$ ratios compared to Class 1 sources because they are early in their accretion stage, and the rotating disk is small in size (Curtis et al. 2010). Thus, it is possible that ^{13}CO molecular detections were faint because CARMA-7's disk is underdeveloped. Alternatively, ^{13}CO emission may be optically thick in this young source, limiting molecular detections near the source.

The lack of clear signs of disk rotation, however, is intriguing given CARMA-7's spectacular outflows. Accretion events are a necessary counterparts to the powerful jets driven by CARMA-7, and therefore, a more developed rotating disk was expected. Here, we find that the strong outflows do not guarantee the presence of an evolved circumstellar disk.

5.4. *Categorizing Gas Tracers*

Given the weak ^{13}CO, N_2D^+ detections and compact 13 CS, and DCN emission features, we are unable to definitively categorize these molecules as tracers of a specific protostellar region. However, we categorize the remaining observed molecular lines as follows:

Outflow	Envelope/Disk	Cavity Wall
CO 2→1	$C^{18}O$ 2→1	c-C_3H_2
H_2CO 3(0,3)-2(0,2)		
H_2CO 3(2,1)-2(2,0)		

Future steps will include identifying accretion flow and streamer tracers as mentioned in Section 5.2.

6. CONCLUSION

In this work, we have analyzed the emission features of 9 molecular lines near the Class 0 protostar, CARMA-7 (Table 1). Our findings can be summarized as follows:

1. The kinematics of the $C^{18}O$ emission features revealed early signs of Keplerian rotation. However, disk and envelope tracers such as ^{13}CO and N_2D^+ were low in abundance and revealed no signs of rotation. We interpret this as an underdeveloped accretion disk that was too small to be detected. Thus, we conclude that CARMA-7 harbors a disk no larger than 305 Au.

2. An extended emission feature was detected at low velocities in the H_2CO 3(0,3)-2(0,2) line. We believe this feature may be an accretion flow, but further analysis is necessary to confirm its origin. Future steps include modeling streamers and examining observations of known accretion flow tracers such as SO.

3. Despite CARMA-7's energetic outflows, there lacks clear evidence of a rotating disk. This reveals that the relationship between accretion events and ejection events is complex and that a strong outflow is not an obvious indicator of an evolved disk.

4. We confirm CO and H_2CO to be outflow gas tracers. $C^{18}O$ emission features traced the envelope and disk. Finally, we identify c-C_3H_2 as an outflow cavity wall tracer.

REFERENCES

Curtis, E. I., Richer, J. S., Swift, J. J., & Williams, J. P. 2010, Monthly Notices of the Royal Astronomical Society, 408, 1516–1539, doi: 10.1111/j.1365-2966.2010.17214.x

Froebrich, D., Schmeja, S., Smith, M., & Klessen, R. 2006, Monthly Notices of the Royal Astronomical Society, 368, 435 , doi: 10.1111/j.1365-2966.2006.10124.x

Hsieh, C.-H., Lai, S.-P., Cheong, P.-I., et al. 2020, ApJ, 894, 23, doi: 10.3847/1538-4357/ab7b69

Larson, R. B. 2003, Reports on Progress in Physics, 66, 1651, doi: 10.1088/0034-4885/66/10/R03

Maret, S., Maury, A. J., Belloche, A., et al. 2020, Astronomy Astrophysics, 635, A15, doi: 10.1051/0004-6361/201936798

Okoda, Y., Oya, Y., Francis, L., et al. 2021, The Astrophysical Journal, 910, 11, doi: 10.3847/1538-4357/abddb1

Pineda, J. E., Segura-Cox, D., Caselli, P., et al. 2020, Nature Astronomy, 4, 1158, doi: 10.1038/s41550-020-1150-z

Plunkett, A. L., Arce, H. G., Mardones, D., et al. 2015, Nature, 527, 70, doi: 10.1038/nature15702

Plunkett, A. L., Fernández-López, M., Arce, H. G., et al. 2018, Astronomy Astrophysics, 615, A9, doi: 10.1051/0004-6361/201732372

Rosolowsky, E. W., Pineda, J. E., Kauffmann, J., & Goodman, A. A. 2008, ApJ, 679, 1338, doi: 10.1086/587685

Sandford, S. A., & Allamandola, L. J. 1993, ApJ, 417, 815, doi: 10.1086/173362

Tobin, J. J., Hartmann, L., Chiang, H.-F., et al. 2012, Nature, 492, 83, doi: 10.1038/nature11610

Tychoniec, L., van Dishoeck, E. F., van 't Hoff, M. L. R., et al. 2021, Which molecule traces what: chemical diagnostics of protostellar sources. https://arxiv.org/abs/2107.03696

Yen, H.-W., Takakuwa, S., Ohashi, N., et al. 2014, The Astrophysical Journal, 793, 1, doi: 10.1088/0004-637x/793/1/1

Yen, H.-W., Takakuwa, S., Chu, Y.-H., et al. 2017, A&A, 608, A134, doi: 10.1051/0004-6361/201730894